

Global Optimization with A Power-Transformed Objective and Gaussian Smoothing

Chen Xu¹

¹Department of Engineering, Shenzhen MSU-BIT University, China.
Email: xuchen@smbu.edu.cn

Abstract

We propose a novel method that solves global optimization problems in two steps: (1) perform a (exponential) power- N transformation to the not-necessarily differentiable objective function f and get f_N , and (2) optimize the Gaussian-smoothed f_N with stochastic approximations. Under mild conditions on f , for any $\delta > 0$, we prove that with a sufficiently large power N_δ , this method converges to a solution in the δ -neighborhood of f 's global optimum point. The convergence rate is $O(d^2\sigma^4\varepsilon^{-2})$, which is faster than both the standard and single-loop homotopy methods if σ is pre-selected to be in $(0, 1)$. In most of the experiments performed, our method produces better solutions than other algorithms that also apply smoothing techniques.

Keywords: Gaussian Smoothing, Homotopy for Optimizations, Adversarial Image Attacks.

1 Introduction

In this work, we consider the global optimization problem of

$$\max_{\mathbf{x} \in \mathcal{S} \subset \mathbb{R}^d} f(\mathbf{x}), \quad (1)$$

where $f(\mathbf{x})$ is a continuous and possibly non-concave function with a global maximum $f(\mathbf{x}^*) > \sup_{\mathbf{x} \neq \mathbf{x}^*} f(\mathbf{x})$, and d is a positive integer. The minimize-version of this problem is often encountered in machine learning, such as model training and adversarial attack in computer vision. The gradient-based algorithms, such as the (stochastic) gradient descent, are commonly used, which only guarantee to approximate a locally optimal solution in a general case.

Homotopy, also called graduated continuation, is a class of methods for finding a global solution to (1), with many successful applications in machine learning (e.g., [22, 10]). It converts the original problem to

$$\max_{\boldsymbol{\mu} \in \mathbb{R}^d, \sigma \geq 0} \mathbb{E}_\xi[f(\boldsymbol{\mu} + \sigma\xi)], \quad (2)$$

where $\sigma \geq 0$ is called the scaling coefficient and ξ is a random variable with a pre-selected distribution, such as a standard multivariate Gaussian distribution (Gaussian Homotopy, GH) or a uniform distribution in a unit sphere. Based on the observation that $\boldsymbol{\mu}_\sigma^* :=$

$\arg \max_{\boldsymbol{\mu}} \mathbb{E}[f(\boldsymbol{\mu} + \sigma\xi)]$ approaches¹ \boldsymbol{x}^* as σ decreases to 0, the homotopy method admits a double-loop mechanism: the outer loop iteratively decreases σ , and for each fixed value of σ , the inner loop solves $\max_{\boldsymbol{\mu}} \mathbb{E}[f(\boldsymbol{\mu} + \sigma\xi)]$, with the solution found in the current inner loop as the starting search point in the next inner loop.

The double-loop mechanism of the homotopy method is costly in time. To tackle this issue, [10] propose a single-loop Gaussian homotopy (SLGH) method that iteratively performs one-step update of $\boldsymbol{\mu}$ and σ , which reduces the convergence rate from $O(d^2/\epsilon^4)$ to $O(d/\epsilon^2)$. However, in theory, SLGH only guarantees to approximate a local optimum², which is not necessarily a global one. A time-efficient algorithm that aims at the global maximum is still to be found.

Therefore, in this work, we propose a new method, namely the Gaussian Smoothing with a Power-transformed Objective (GSPTO), for solving the optimization problem of (1). According to our Corollary 1, GSPTO converges to a neighborhood of \boldsymbol{x}^* with the rate of $O(d^2\sigma^4/\epsilon^2)$. It indicates that GSPTO is faster than the standard homotopy and SLGH, if $\sigma > 0$ is pre-selected to be in $(0, 1)$. Most of the experiments in Section 5 show that the GSPTO-based algorithm (e.g., EPGS, introduced later) outperforms other algorithms that also apply the smoothing technique.

Motivation

Under the condition of $\int_{\mathbb{R}^d} f(\boldsymbol{x})d\boldsymbol{x} > 0$ and an additional one, there is a threshold $\sigma_m > 0$ such that whenever $\sigma > \sigma_m$, the Gaussian-smoothed objective $E_{\boldsymbol{\xi} \sim \mathcal{N}(\mathbf{0}, I_d)}[f(\boldsymbol{\mu} + \sigma\boldsymbol{\xi})]$ is concave in $\boldsymbol{\mu}$ (see [17, Main Result (Corollary 9)]). Hence, Gaussian smoothing converts the original possibly non-concave maximization problem to a concave one, if the maximum point $\boldsymbol{\mu}^*$ coincides with \boldsymbol{x}^* . Although this condition is not true in general³, we can modify the objective to make $\boldsymbol{\mu}^*$ close to \boldsymbol{x}^* , where recall that \boldsymbol{x}^* denotes the global maximum point of the original objective f before modification.

Intuitively, if we modify $f(\boldsymbol{x})$ to put sufficiently large weight on its global maximum \boldsymbol{x}^* , the global maximum $\boldsymbol{\mu}^* := \arg \max_{\boldsymbol{\mu}} F(\boldsymbol{\mu}, \sigma)$ should get close enough to \boldsymbol{x}^* . One way of such modification is by taking powers of f , if $f(\boldsymbol{x}^*) > 1$. The difference $f^N(\boldsymbol{x}^*) - f^N(\boldsymbol{x})$ is positively related with the power N , which indicates that more weight is put on \boldsymbol{x}^* as N increases. Figure 1(a) verifies this intuition with an example, and Figure 1(b) illustrates the effects of taking exponential powers. As shown in these two toy examples, $\boldsymbol{\mu}^*$ approaches \boldsymbol{x}^* as N increases.

From the above intuition, we propose GSPTO for solving the global optimization problem (1), which is a new method that places more weight on the objective f 's maximum value (by increasing the gap between the global and local maximum values) before performing Gaussian smoothing. Based on GSPTO, we design two algorithms⁴, Power Gaussian Smoothing (PGS) and Exponential Power Gaussian Smoothing (EPGS), which are featured with replacing the original objective $f(\boldsymbol{x})$ with a (exponential) power transformation. Specifically, with σ and N as two hyper-parameters, PGS solves $\max_{\boldsymbol{\mu}} \mathbb{E}_{\boldsymbol{x} \sim \mathcal{N}(\boldsymbol{\mu}, \sigma^2 I_d)}[f^N(\boldsymbol{x})]$ and EPGS solves $\max_{\boldsymbol{\mu}} \mathbb{E}_{\boldsymbol{x} \sim \mathcal{N}(\boldsymbol{\mu}, \sigma^2 I_d)}[e^{Nf(\boldsymbol{x})}]$, both using a stochastic gradient ascent algorithm derived in this paper, which does not require the differentiability of f . Here, \mathcal{N} denotes a multivariate Gaussian distribution and I_d denotes an identity matrix of dimension $d \times d$.

¹Note that $\mathbb{E}[f(\boldsymbol{\mu} + \sigma\xi)] = f(\boldsymbol{\mu})$ if $\sigma = 0$.

²Theorem 4.1 in [10] shows that SLGH approximates a solution $\hat{\boldsymbol{x}}$ such that $\mathbb{E}[\nabla f(\hat{\boldsymbol{x}})] = 0$.

³This is why smoothing alone is insufficient for optimization, and is typically used in conjunction with iteratively reducing the scaling parameter, which becomes the homotopy algorithm.

⁴See Algorithm 1 for the two algorithms.

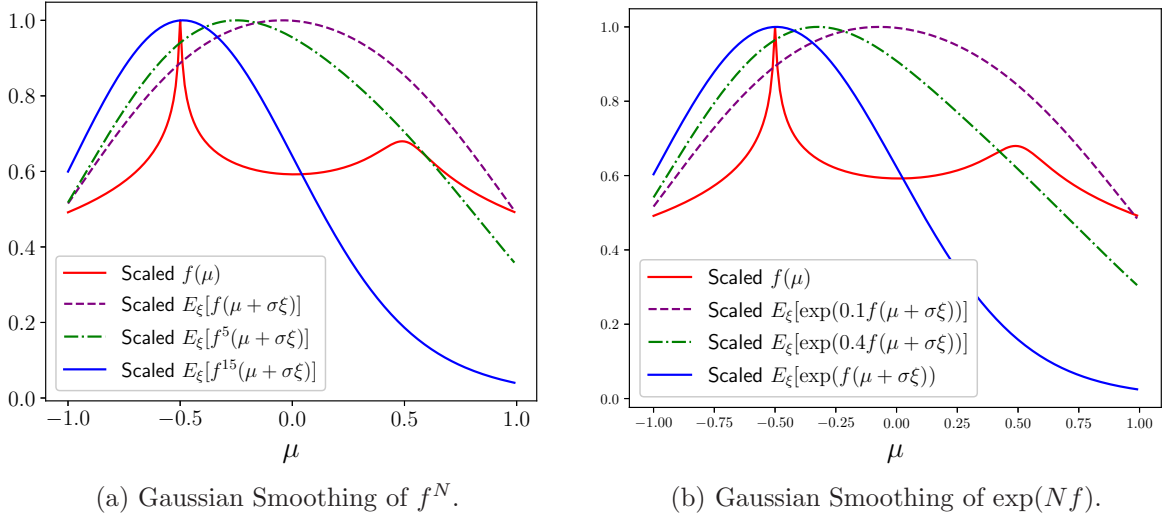


Figure 1: Effects of elevating the objective f before Gaussian smoothing (A toy example): The maximum point of $F_N(\mu) := \mathbb{E}_{\xi \sim \mathcal{N}(0,1)}[f_N(\mu + \sigma\xi)]$ gets closer to the global maximum point f as N increases, where $\sigma = 0.5$ and $f(\mu) = -\log((\mu+0.5)^2 + 10^{-5}) - \log((\mu+0.5)^2 + 10^{-2}) + 10$ for $|\mu| \leq 1$ and $f(\mu) = 0$ for $|\mu| > 1$. For easier comparison, the graph of each function is scaled to have a maximum value of 1.

Related Work

The homotopy methods, firstly proposed in [2, Chapter 7], are intensively studied in the field of machine learning for global optimization problems. [16] derives a bound for the worst scenario of the GH algorithm in a deterministic setting (i.e., the expectation \mathbb{E} is not approximated with samples), while [9] provides a convergence analysis in a stochastic setting (i.e., \mathbb{E} is estimated with samples). Specifically, the latter proves that with a probability greater than $1 - p$, the solution $\hat{\mathbf{x}}$ produced by their proposed homotopy algorithm is ϵ -optimal (i.e., $f(\mathbf{x}^*) - f(\hat{\mathbf{x}}) < \epsilon$) after $\tilde{O}(d^2/(\sigma^2\epsilon^4))$ steps of solution-update. [7] changes the distribution of the perturbation ξ from the commonly used Gaussian or uniform to the distribution that minimizes the estimation error of the gradient $\nabla_{\mu} E_{\xi \sim \mathcal{N}(0, I_d)}[f(\mu + \sigma\xi)]$. [13] proposes an algorithm for learning the whole solution path produced by the homotopy. Specifically, their algorithm learns a model $x_{\phi}(\sigma)$ that predicts (for any $\sigma > 0$) the solution to $\min_{\mu} \nabla_{\mu} E_{\xi \sim \mathcal{N}(0, I_d)}[f(\mu + \sigma\xi)]$, where ϕ is the set of model parameters to be trained.

The smoothing and homotopy methods have a large number of successful applications in machine learning, such as neural network training ([9]), adversarial attack on image classification models ([10]), solving L_1 -regularized least-square problems ([21]), neural combinatorial optimization ([7]), improving the optimization algorithms of stochastic gradient descent and Adam ([20]), and so on.

There are a few existing studies ([6, 19, 4]) that replace the original f with a surrogate objective that also involves the exponential transformation $e^{Nf(\mu+\xi)}$ before smoothing. But their works are different from ours. [6] propose to minimize the surrogate objective of $G(\mu) := \frac{1}{N} \log(\mathbb{E}_{\xi \sim \mathcal{N}(0, \Sigma)}[e^{Nf(\mu+\xi)}]) + \frac{1}{2} \mu^T R \mu$. The theory⁵ that justifies this surrogate objective requires that N, R , and Σ be selected so that $NR - \Sigma^{-1}$ is positive semi-definite. This indicates that EPGS, for which $R = \mathbf{0}$ and $\Sigma = \sigma I_d$, is not a special case of theirs, since $-\sigma^{-1} I_d$ is negative definite and violates their requirement. Moreover, their theory on the distance between the optimum point of the new surrogate and \mathbf{x}^* is incomplete (see [6, Section 3.2]). For optimal-control problems, [19] study the surrogate objective that

⁵ $\min_{\mu} G(\mu, \Sigma)$ is a convex problem given that $NR - \Sigma^{-1}$ is positive definite and \mathcal{C} is convex ([6, Theorem 3.1]).

is similar to $G(\boldsymbol{\mu})$, and provide a theoretical analysis on the corresponding algorithm’s convergence to a stationary point. However, the relation between this stationary point and the global optimum point \boldsymbol{x}^* is not revealed. The proposed surrogate objective in [4] is $(1 - N)f(\boldsymbol{\mu}) + \log(\mathbb{E}_{\xi \sim \mathcal{N}(0, \Sigma)}[e^{Nf(\boldsymbol{\mu} + \xi)}])$, where $N \in [0, 1]$. This is very different from GSPTO’s requirement that N is sufficiently large. Also, their theory ([4, Theorem 10]) bounds $|f(\boldsymbol{x}^*) - f(\boldsymbol{\mu}^*)|$ with $O(N\sigma^2)$, which does not imply an improvement for increasing the value of N .

Contribution

This paper introduces a novel method, GSPTO, for solving global optimization problems, with the contributions summarized as follows.

1. To our knowledge, for global optimization problems, this is the first work that proposes the idea⁶ of putting sufficiently large weight on the global maximum values of the objective, to decrease the distance between the optimum point before and after Gaussian smoothing (i.e., $\|\boldsymbol{x}^* - \boldsymbol{\mu}^*\|$). PGS and EPGS are two ways of realizing this idea, and future studies are motivated for finding better ones.
2. In theory, GSPTO is faster than the homotopy methods for optimization. According to Corollary 1, GSPTO has a convergence rate of $O(d^2\sigma^4\varepsilon^{-2})$, which is faster than the standard homotopy method ($O(d^2\sigma^{-2}\varepsilon^{-4})$, [9, Theorem 5.1]), and SLGH ($O(d^2\varepsilon^{-2})$, [10, Theorem 4.1]), if σ is pre-selected to be in $(0, 1)$. Most of our experiments show that it outperforms other optimization algorithms that also apply the smoothing technique (see Section 5.4).
3. Our convergence analysis does not require the Lipschitz condition on the original objective f , which is assumed in the theoretical analysis of homotopy methods in other studies ([9, 10]). Therefore, our analysis applies to more situations.
4. The theory derived in this work is on the distance between the found solution and the optimal one, while the convergence analysis in other studies on homotopy (e.g., [9, 10]) is on the objective value of the found solution. Therefore, our theory has a wider range of applications (e.g., for problems that concern the distance between the found solution and the optimal like inverse problems and adversarial attack in image recognition).

2 Preliminaries

We rigorously prove the intuition that motivates GSPTO: Given $\sigma > 0$, for any $\delta > 0$, there exists a threshold such that whenever N exceeds this threshold, the global maximum point of $F_N(\boldsymbol{\mu}, \sigma)$ lies within a δ -neighborhood of \boldsymbol{x}^* , where $F_N(\boldsymbol{\mu}) := \mathbb{E}_{\boldsymbol{x} \sim \mathcal{N}(\boldsymbol{\mu}, \sigma I_d)}[f_N(\boldsymbol{x})]$, and

$$\begin{aligned}
 f_N(\boldsymbol{x}_k) &:= \begin{cases} f^N(\boldsymbol{x}_k), & \boldsymbol{x} \in \mathcal{S}; \\ 0, & \text{otherwise,} \end{cases} & \text{(PGS setting);} \\
 f_N(\boldsymbol{x}_k) &:= \begin{cases} e^{Nf(\boldsymbol{x}_k)}, & \boldsymbol{x} \in \mathcal{S}; \\ 0, & \text{otherwise.} \end{cases} & \text{(EPGS setting).}
 \end{aligned} \tag{3}$$

⁶[6], [19], and [4] have not mentioned this idea.

Theorem 1. Let $f : \mathcal{S} \subset \mathbb{R}^d \rightarrow \mathbb{R}$ be a continuous function that is possibly non-concave (and non-negative only for the case of PGS), where \mathcal{S} is compact. Assume that f has a global maximum \mathbf{x}^* such that $\sup_{\mathbf{x} : \|\mathbf{x} - \mathbf{x}^*\| \geq \delta} f(\mathbf{x}) < f(\mathbf{x}^*)$ for any $\delta > 0$. For $\sigma > 0$, define

$$F_N(\boldsymbol{\mu}, \sigma) := (\sqrt{2\pi}\sigma)^{-k} \int_{\mathbf{x} \in \mathbb{R}^k} f_N(\mathbf{x}) e^{-\frac{\|\mathbf{x} - \boldsymbol{\mu}\|^2}{2\sigma^2}} d\mathbf{x}, \quad N \in \{0, 1, 2, \dots\},$$

where f_N is defined in (3) for either PGS or EPGS. Then, for any $M > 0$ and $\delta > 0$ such that $\bar{B}(\mathbf{x}^*; \delta) := \{\mathbf{x} \in \mathbb{R}^d : \|\mathbf{x} - \mathbf{x}^*\| \leq \delta\} \subset \mathcal{S}$, there exists $N_{\delta, \sigma, M} > 0$, such that whenever $N > N_{\delta, \sigma, M}$, we have for any $\|\boldsymbol{\mu}\| < M$ that: $\frac{\partial F_N(\boldsymbol{\mu}, \sigma)}{\partial \mu_i} > 0$ if $\mu_i < x_i^* - \delta$, and $\frac{\partial F_N(\boldsymbol{\mu}, \sigma)}{\partial \mu_i} < 0$ if $\mu_i > x_i^* + \delta$. Here, μ_i and x_i^* denote the i^{th} entry of $\boldsymbol{\mu}$ and \mathbf{x}^* , respectively, where $i \in \{1, 2, \dots, d\}$.

Proof. See the appendix for the proof for the EPGS setting. The proof for the PGS setting is similar. \square

3 Gaussian Smoothing with Power-Transformed Objective

3.1 The Solution Updating Rule

For the optimization problem (1), based on Theorem 1, with the pre-selected hyperparameters N and $\sigma > 0$, GSPTO follows a stochastic gradient ascent scheme to solve $\max_{\boldsymbol{\mu}} F_N(\boldsymbol{\mu}, \sigma)$. Specifically, the rule for updating the solution candidate used is

$$\text{GSPTO :} \quad \boldsymbol{\mu}_{t+1} = \boldsymbol{\mu}_t + \alpha_t \hat{\nabla} F_N(\boldsymbol{\mu}_t), \quad (4)$$

where $\hat{\nabla}_{\boldsymbol{\mu}} F(\boldsymbol{\mu}_t) := \frac{1}{K} \sum_{k=1}^K (\mathbf{x}_k - \boldsymbol{\mu}_t) f_N(\mathbf{x}_k)$, $\{\mathbf{x}_k\}_{k=1}^K$ are independently sampled from the multivariate Gaussian distribution $\mathcal{N}(\boldsymbol{\mu}, \sigma^2 I_d)$, and $f_N(\mathbf{x}_k)$ is defined in (3). Note that $\widehat{\nabla} F_N(\boldsymbol{\mu}_t)$ is a sample estimate of the gradient $\nabla F(\boldsymbol{\mu}_t)$:

$$\begin{aligned} \nabla_{\boldsymbol{\mu}} F(\boldsymbol{\mu}_t) &= \nabla_{\boldsymbol{\mu}} \mathbb{E}_{\mathbf{x} \sim \mathcal{N}(\boldsymbol{\mu}, \sigma^2 I_d)} [f_N(\mathbf{x})] \\ &= (\sqrt{2\pi}\sigma)^{-1} \int_{\mathbf{x} \in B(\mathbf{0}; M)} (\mathbf{x} - \boldsymbol{\mu}_t) f_N(\mathbf{x}) e^{-\frac{\|\mathbf{x} - \boldsymbol{\mu}_t\|^2}{2\sigma^2}} d\mathbf{x}. \\ &= \mathbb{E}_{\mathbf{x} \sim \mathcal{N}(\boldsymbol{\mu}, \sigma I_d)} [(\mathbf{x} - \boldsymbol{\mu}_t) f_N(\mathbf{x})]. \end{aligned}$$

Based on GSPTO, PGS and EPGS are designed in Algorithm 1. They normalize the gradient before updating the solution, which is a common practice to stabilize results.

Remark 1. An effective method to avoid computation overflows caused by a large N -value is to modify the gradient estimate as

$$\hat{\nabla}_{\boldsymbol{\mu}} F(\boldsymbol{\mu}_t) := \begin{cases} \frac{1}{K} \sum_{k=1}^K (\mathbf{x}_k - \boldsymbol{\mu}_k) f_N(\mathbf{x}_k) f^N(\mathbf{x}_k) / f^N(\boldsymbol{\mu}_t), & \text{for PGS;} \\ \frac{1}{K} \sum_{k=1}^K (\mathbf{x}_k - \boldsymbol{\mu}_k) f_N(\mathbf{x}_k) e^{N(f(\mathbf{x}_k) - f(\boldsymbol{\mu}_t))}, & \text{for EPGS.} \end{cases}$$

This modification produces the same $\boldsymbol{\mu}$ -updates as in Algorithm 1 because of the gradient-normalization step.

4 Convergence Analysis

We perform convergence analysis for the updating rule (4) under the PGS and EPGS setting (3) on the optimization problem of (1). We show that, for any $\varepsilon > 0$ and any $\delta > 0$, GSPTO converges to a δ -neighborhood of \mathbf{x}^* with the iteration complexity of $O(d^2 \sigma^4 \varepsilon^{-2})$. Specifically, with $T = O((d\sigma^2)^{2/(1-2\gamma)} \varepsilon^{-2/(1-2\gamma)})$ times of updating $\boldsymbol{\mu}_t$, $\mathbb{E}[\|\nabla F(\boldsymbol{\mu}_T)\|^2] < \varepsilon$, where γ can be arbitrarily close to 0. The result is summarized in Corollary 1.

Algorithm 1: PGS/EPGS

Require: The power $N > 0$, the scaling parameter $\sigma > 0$, the objective f , the initial value $\boldsymbol{\mu}_0$, the number K of sampled points for gradient approximation, the total number T of $\boldsymbol{\mu}$ -updates, and the learning rate schedule $\{\alpha_t\}_{t=1}^T$.

Result: $\boldsymbol{\mu}_T$ - The approximated solution to (1).

for t from 0 to $T-1$ **do**

Independently sample from $\mathcal{N}(\boldsymbol{\mu}_t, \sigma I_d)$ (multivariate Gaussian distribution), and obtain $\{\mathbf{x}_k\}_{k=1}^K$.

$\boldsymbol{\mu}_{t+1} = \boldsymbol{\mu}_t + \alpha_t \widehat{\nabla F_N}(\boldsymbol{\mu}_t) / \|\widehat{\nabla F_N}(\boldsymbol{\mu}_t)\|$, where

$\widehat{\nabla}_{\boldsymbol{\mu}} F(\boldsymbol{\mu}_t) := \frac{1}{K} \sum_{k=1}^K (\mathbf{x}_k - \boldsymbol{\mu}_t) f_N(\mathbf{x}_k)$ and $f_N(\mathbf{x}_k) := \begin{cases} f^N(\mathbf{x}_k), & \text{for PGS;} \\ e^{Nf(\mathbf{x}_k)}, & \text{for EP GS.} \end{cases}$

end

Return($\boldsymbol{\mu}_T$).

4.1 Notation

In this section, let $\delta > 0$ and $\sigma > 0$ be fixed, and $\delta > 0$ satisfies

$$\mathcal{S}_{\mathbf{x}^*, \delta} := \{\boldsymbol{\mu} \in \mathbb{R}^d : |\mu_i - x_i^*| \leq \delta, \text{ for each } i \in \{1, 2, \dots, d\}\} \subset \mathcal{S}, \quad (5)$$

where i denotes the i^{th} entry and \mathcal{S} is specified in Assumption 1. Let $N > 0$ be such that for any $\|\boldsymbol{\mu}\| \leq \sqrt{d}M$: $\frac{\partial F_N(\boldsymbol{\mu}, \sigma)}{\partial \mu_i} > 0$ if $\mu_i < x_i^* - \delta$, and $\frac{\partial F_N(\boldsymbol{\mu}, \sigma)}{\partial \mu_i} < 0$ if $\mu_i > x_i^* + \delta$, for all $i \in \{1, 2, \dots, d\}$. Such an N exists because of Theorem 1. Here, M is specified in Assumption 1. Let $F_N(\boldsymbol{\mu}, \sigma)$ be as defined as in Theorem 1. Unless needed, we omit N and σ in this symbol as they remain fixed in this section, and write $F(\boldsymbol{\mu})$ instead. $\nabla F(\boldsymbol{\mu})$ refers to the gradient of F with respect to $\boldsymbol{\mu}$. Let f_N be defined as in (3).

4.2 Assumptions and Lemmas

Assumption 1. Assume that $f(\mathbf{x}) : \mathcal{S} \rightarrow \mathbb{R}$ is a function satisfying the conditions specified in Theorem 1, where $\mathcal{S} \subset \mathcal{S}_M := \{\mathbf{x} \in \mathbb{R}^d : |x_i| \leq M, i \in \{1, 2, \dots, d\}\}$, for some $M > 0$. Also, $\|F(\boldsymbol{\mu})\|, \|\nabla F(\boldsymbol{\mu})\| < +\infty$ for all $\boldsymbol{\mu} \in \mathbb{R}^d$.

Assumption 2. Assume that the learning rate α_t satisfies

$$\alpha_t > 0, \quad \sum_{t=0}^{\infty} \alpha_t = +\infty, \quad \text{and} \quad \sum_{t=0}^{\infty} \alpha_t^2 < +\infty.$$

Lemma 1. Under Assumption 1, any local or global maximum point $\boldsymbol{\mu}^*$ of $F(\boldsymbol{\mu})$ belongs to $\mathcal{S}_{\mathbf{x}^*, \delta}$, which is defined in (5).

Proof. For any point $\boldsymbol{\mu} \notin \mathcal{S}_{\mathbf{x}^*, \delta}$, we show that $\nabla F(\boldsymbol{\mu}) \neq 0$. If $\boldsymbol{\mu} \in \mathcal{S}_M - \mathcal{S}_{\mathbf{x}^*, \delta}$, then $\|\boldsymbol{\mu}\| \leq \sqrt{d}M$ and there is some $j \in \{1, 2, \dots, d\}$ such that $|\mu_j - x_j^*| > \delta$, which implies $\frac{\partial F(\boldsymbol{\mu})}{\partial \mu_j} \neq 0$ because of the definition of N in Section 4.1.

On the other hand, if $\boldsymbol{\mu} \notin \mathcal{S}_M$, there is at least one j such that $|\mu_j| > M$. Then,

$$\begin{aligned} \frac{\partial F(\boldsymbol{\mu})}{\partial \mu_j} &= \frac{1}{(\sqrt{2\pi})^k \sigma^{k+2}} \int_{\mathbf{x} \in \mathbb{R}^d} (x_j - \mu_j) e^{-\frac{\|\mathbf{x} - \boldsymbol{\mu}\|^2}{2\sigma^2}} f_N(\mathbf{x}) d\mathbf{x} \\ &= \frac{1}{(\sqrt{2\pi})^k \sigma^{k+2}} \int_{\mathbf{x} \in \mathcal{S}} (x_j - \mu_j) e^{-\frac{\|\mathbf{x} - \boldsymbol{\mu}\|^2}{2\sigma^2}} f_N(\mathbf{x}) d\mathbf{x}, \text{ by def. of } f_N \text{ in (3),} \\ &= \begin{cases} \text{negative,} & \text{if } \mu_j > M; \\ \text{positive,} & \text{if } \mu_j < -M. \end{cases}, \text{ since } x_j \in \mathcal{S} \Rightarrow |x_j| \leq M \text{ by Assumption 1.} \end{aligned}$$

In sum, for any point $\boldsymbol{\mu} \notin \mathcal{S}_{\mathbf{x}^*, \delta}$, $\nabla F(\boldsymbol{\mu}) \neq 0$, which further implies that any local or global maximum point $\boldsymbol{\mu}^*$ of $F(\boldsymbol{\mu})$ belongs to $\mathcal{S}_{\mathbf{x}^*, \delta}$ since $\nabla F(\boldsymbol{\mu}^*) = 0$. \square

Lemma 2. *Under Assumption 1, for any $\sigma > 0$, the objective function $F_N(\boldsymbol{\mu}, \sigma)$ is Lipschitz Smooth. That is, for any $\boldsymbol{\mu}_1, \boldsymbol{\mu}_2 \in \mathbb{R}^d$,*

$$\|\nabla F_N(\boldsymbol{\mu}_1, \sigma) - \nabla F_N(\boldsymbol{\mu}_2, \sigma)\| \leq L\|\boldsymbol{\mu}_1 - \boldsymbol{\mu}_2\|,$$

where $L = f^N(\mathbf{x}^*)$ for the case of PGS and $L = e^{Nf(\mathbf{x}^*)}$ for the case of EPGS.

Proof. $F_N(\boldsymbol{\mu}, \sigma) = \mathbb{E}_{\mathbf{x} \sim \mathcal{N}(\boldsymbol{\mu}, \sigma^2 I_d)}[f_N(\mathbf{x})]$, where $f_N(\mathbf{x})$ is as defined in (3). $\nabla_{\boldsymbol{\mu}} F_N(\boldsymbol{\mu}, \sigma) = \mathbb{E}_{\mathbf{x} \sim \mathcal{N}(\boldsymbol{\mu}, \sigma^2 I_d)}[(\mathbf{x} - \boldsymbol{\mu})f_N(\mathbf{x})]$. Then,

$$\|\nabla F_N(\boldsymbol{\mu}_1, \sigma) - \nabla F_N(\boldsymbol{\mu}_2, \sigma)\| = \|\mathbb{E}_{\mathbf{x} \sim \mathcal{N}(\boldsymbol{\mu}, \sigma^2 I_d)}[(\boldsymbol{\mu}_1 - \boldsymbol{\mu}_2)f_N(\mathbf{x})]\| \leq \|\boldsymbol{\mu}_1 - \boldsymbol{\mu}_2\|f_N(\mathbf{x}^*).$$

Hence, $L = f_N(\mathbf{x}^*)$, which is $f^N(\mathbf{x}^*)$ for PGS and $L = e^{Nf(\mathbf{x}^*)}$ for EPGS. \square

Lemma 3. *Under Assumption 1, for any $\sigma > 0$, let $\hat{\nabla}_{\boldsymbol{\mu}} F_N(\boldsymbol{\mu}, \sigma)$ be defined in (4). Then, $\mathbb{E}[\|\hat{\nabla}_{\boldsymbol{\mu}} F_N(\boldsymbol{\mu}, \sigma)\|^2] < G$, where*

$$G = \begin{cases} d\sigma^2 f^{2N}(\mathbf{x}^*), & \text{for PGS;} \\ d\sigma^2 e^{2Nf(\mathbf{x}^*)}, & \text{for EPGS.} \end{cases}$$

Proof.

$$\begin{aligned} \mathbb{E} \left[\|\hat{\nabla} F_N(\boldsymbol{\mu}_t)\|^2 \right] &= \frac{1}{K^2} \sum_{k=1}^K \sum_{l=1}^K \mathbb{E}_{\mathbf{x}_k, \mathbf{x}_l \sim \mathcal{N}(\boldsymbol{\mu}_t, \sigma^2 I_d)} [(\mathbf{x}_k - \boldsymbol{\mu}_t)'(\mathbf{x}_l - \boldsymbol{\mu}_t) f_N(\mathbf{x}_k) f_N(\mathbf{x}_l)] \\ &\leq f_N^2(\mathbf{x}^*) \frac{1}{K^2} \sum_{k=1}^K \sum_{l=1}^K \mathbb{E}_{\mathbf{x}_k, \mathbf{x}_l \sim \mathcal{N}(\boldsymbol{\mu}_t, \sigma^2 I_d)} [|(\mathbf{x}_k - \boldsymbol{\mu}_t)'(\mathbf{x}_l - \boldsymbol{\mu}_t)|] \\ &\leq f_N^2(\mathbf{x}^*) \frac{1}{K^2} \sum_{k=1}^K \sum_{l=1}^K \mathbb{E}_{\mathbf{x}_k, \mathbf{x}_l \sim \mathcal{N}(\boldsymbol{\mu}_t, \sigma^2 I_d)} [\|(\mathbf{x}_k - \boldsymbol{\mu}_t)\| \cdot \|(\mathbf{x}_l - \boldsymbol{\mu}_t)\|], \\ &\leq f_N^2(\mathbf{x}^*) \frac{1}{K^2} \sum_{k=1}^K \sum_{l=1}^K \sqrt{\mathbb{E}[\|\mathbf{x}_k - \boldsymbol{\mu}_t\|^2] \mathbb{E}[\|\mathbf{x}_l - \boldsymbol{\mu}_t\|^2]}, \quad \text{by Schwarz Ineq.,} \\ &= f_N^2(\mathbf{x}^*) \sigma^2 d, \quad d \text{ denotes the number of dimensions,} \end{aligned}$$

where the third line is by Cauchy-Schwarz Inequality. Replacing $f_N^2(\mathbf{x}^*) = e^{2Nf(\mathbf{x}^*)}$ for EPGS and $f_N^2(\mathbf{x}^*) = f^{2N}(\mathbf{x}^*)$ for PGS gives the desired result. \square

4.3 Convergence Rate

Theorem 2. *Let $\{\boldsymbol{\mu}_t\}_{t=0}^T \subset \mathbb{R}^d$ be produced by following the iteration rule of (4), with a pre-selected and deterministic $\boldsymbol{\mu}_0$ and all the involved terms defined as in Section 4.1. Then, under Assumption 1 and 2, we have that*

$$\sum_{t=0}^{T-1} \alpha_t \mathbb{E}[\|\nabla F(\boldsymbol{\mu}_t)\|^2] \leq f(\mathbf{x}^*) - F(\boldsymbol{\mu}_0) + LG \sum_{t=0}^{\infty} \alpha_t^2,$$

where L and G are as defined in Lemma 2 and Lemma 3, respectively.

Remark 2. If $\alpha_t = (t+1)^{-(1/2+\gamma)}$ with $\gamma \in (0, 1/2)$. Then,

$$\frac{f(\mathbf{x}^*) - F(\boldsymbol{\mu}_0) + LG \sum_{t=1}^{\infty} t^{-(1+2\gamma)}}{\sum_{t=1}^T t^{-(1/2+\gamma)}} < \frac{f(\mathbf{x}^*) - F(\boldsymbol{\mu}_0) + LG \sum_{t=1}^{\infty} t^{-(1+2\gamma)}}{\int_1^T t^{-(1/2+\gamma)} dt} = O(d\sigma^2 T^{-1/2+\gamma}),$$

where $d\sigma^2$ comes from G in Lemma 3. This inequality and Theorem 2 implies that after $T = O((d\sigma^2 \varepsilon^{-1})^{2/(1-2\gamma)})$ times of updating $\boldsymbol{\mu}_t$ by GSPTO, $\mathbb{E}[\|\nabla F(\boldsymbol{\mu}_T)\|^2] < \varepsilon$. In sum, the GSPTO method (4) converges to a δ -neighborhood of \mathbf{x}^* with a rate of $O((d\sigma^2 \varepsilon^{-1})^{2/(1-2\gamma)})$, where γ can be arbitrarily close to 0.

Proof. By the Gradient Mean Value Theorem, there exists $\boldsymbol{\nu}_t \in \mathbb{R}^d$ such that $\nu_{t,i}$ lies between $\mu_{t+1,i}$ and $\mu_{t,i}$ for each of the i th entry, and

$$\begin{aligned} F(\boldsymbol{\mu}_{t+1}) &= F(\boldsymbol{\mu}_t) + (\nabla F(\boldsymbol{\nu}_t))'(\boldsymbol{\mu}_{t+1} - \boldsymbol{\mu}_t), \quad ' \text{ denotes matrix transpose,} \\ &= F(\boldsymbol{\mu}_t) + (\nabla F(\boldsymbol{\mu}_t))'(\boldsymbol{\mu}_{t+1} - \boldsymbol{\mu}_t) + (\nabla F(\boldsymbol{\nu}_t) - \nabla F(\boldsymbol{\mu}_t))'(\boldsymbol{\mu}_{t+1} - \boldsymbol{\mu}_t) \\ &= F(\boldsymbol{\mu}_t) + \alpha_t (\nabla F(\boldsymbol{\mu}_t))'(\hat{\nabla} F(\boldsymbol{\mu}_t)) - (\nabla F(\boldsymbol{\mu}_t) - \nabla F(\boldsymbol{\nu}_t))'(\boldsymbol{\mu}_{t+1} - \boldsymbol{\mu}_t) \\ &\geq F(\boldsymbol{\mu}_t) + \alpha_t (\nabla F(\boldsymbol{\mu}_t))'(\hat{\nabla} F(\boldsymbol{\mu}_t)) - L \|\boldsymbol{\nu}_t - \boldsymbol{\mu}_t\| \cdot \|\boldsymbol{\mu}_{t+1} - \boldsymbol{\mu}_t\|, \text{ by Lemma 2,} \\ &\geq F(\boldsymbol{\mu}_t) + \alpha_t (\nabla F(\boldsymbol{\mu}_t))'(\hat{\nabla} F(\boldsymbol{\mu}_t)) - L \|\boldsymbol{\mu}_{t+1} - \boldsymbol{\mu}_t\|^2, \nu_{t,i} \text{ is between } \mu_{t+1,i} \text{ and } \mu_{t,i} \\ &= F(\boldsymbol{\mu}_t) + \alpha_t (\nabla F(\boldsymbol{\mu}_t))'(\hat{\nabla} F(\boldsymbol{\mu}_t)) - \alpha_t^2 L \|\hat{\nabla} F_N(\boldsymbol{\mu}_t)\|^2. \end{aligned}$$

Hence, we have

$$F(\boldsymbol{\mu}_{t+1}) \geq F(\boldsymbol{\mu}_t) + \alpha_t (\nabla F(\boldsymbol{\mu}_t))'(\hat{\nabla} F(\boldsymbol{\mu}_t)) - \alpha_t^2 L \|\hat{\nabla} F_N(\boldsymbol{\mu}_t)\|^2.$$

Taking the expectation of both sides gives

$$\begin{aligned} \mathbb{E}[F(\boldsymbol{\mu}_{t+1})] &\geq \mathbb{E}[F(\boldsymbol{\mu}_t)] + \alpha_t \mathbb{E}[\|\nabla F(\boldsymbol{\mu}_t)\|^2] - \alpha_t^2 L \mathbb{E}[\|\hat{\nabla} F_N(\boldsymbol{\mu}_t)\|^2] \\ &\geq \mathbb{E}[F(\boldsymbol{\mu}_t)] + \alpha_t \mathbb{E}[\|\nabla F(\boldsymbol{\mu}_t)\|^2] - \alpha_t^2 LG, \text{ by Lemma 3,} \end{aligned} \quad (6)$$

where for the first line, note that

$$\mathbb{E}[(\nabla F(\boldsymbol{\mu}_t))'(\hat{\nabla} F(\boldsymbol{\mu}_t))] = \mathbb{E} \left[\mathbb{E}[(\nabla F(\boldsymbol{\mu}_t))'(\hat{\nabla} F(\boldsymbol{\mu}_t)) | \boldsymbol{\mu}_t] \right] = \mathbb{E}[\|\nabla F(\boldsymbol{\mu}_t)\|^2].$$

Taking the sum from $t = 0$ to $t = T - 1$ on both sides of (6) gives

$$\mathbb{E}[F(\boldsymbol{\mu}_T)] \geq \mathbb{E}[F(\boldsymbol{\mu}_0)] + \sum_{t=0}^{T-1} \alpha_t \mathbb{E}[\|\nabla F(\boldsymbol{\mu}_t)\|^2] - LG \sum_{t=0}^{T-1} \alpha_t^2.$$

Re-organizing the terms gives

$$\begin{aligned} \sum_{t=0}^{T-1} \alpha_t \mathbb{E}[\|\nabla F(\boldsymbol{\mu}_t)\|^2] &\leq \mathbb{E}[F(\boldsymbol{\mu}_T)] - \mathbb{E}[F(\boldsymbol{\mu}_0)] + LG \sum_{t=0}^{T-1} \alpha_t^2 \\ &\leq f(\mathbf{x}^*) - F(\boldsymbol{\mu}_0) + LG \sum_{t=0}^{\infty} \alpha_t^2 \end{aligned}$$

This finishes the proof for Theorem 2. \square

We summarize the above results in the following corollary.

Corollary 1. Suppose Assumption 1 and 2 hold. Given any $\delta > 0$ and $\sigma > 0$, there exists $N > 0$ such that $F_N(\boldsymbol{\mu})$ has all its local maximums in $\mathcal{S}_{\mathbf{x}^*, \delta} := \{\boldsymbol{\mu} \in \mathbb{R}^d : |\mu_i - x_i^*| \leq \delta, \text{ for each } i \in \{1, 2, \dots, d\}\}$. For any $\varepsilon > 0$, under either the PGS or EPGS setting, the updating rule (4) of GSPTO produces $\boldsymbol{\mu}_t$ that converges to a local maximum point of $F_N(\boldsymbol{\mu})$, which lies in the δ -neighborhood $\mathcal{S}_{\mathbf{x}^*, \delta}$ of \mathbf{x}^* , with the iteration complexity of $O(d^2 \sigma^4 \varepsilon^{-2})$. Specifically, after $T = O((d\sigma^2 \varepsilon^{-1})^{2/(1-2\gamma)})$ times of $\boldsymbol{\mu}_t$ -updating by (4), $\mathbb{E}[\|\nabla F(\boldsymbol{\mu}_T)\|^2] < \varepsilon$, where $\gamma \in (0, 1/2)$ is a parameter in the learning rate $\alpha_t := (t+1)^{-(1/2+\gamma)}$ and can be arbitrarily close to 0.

5 Experiments

5.1 Effects of Increasing Powers

We illustrate the improvements made by increasing N for PGS/EPGS through an example problem of

$$\max_{\mathbf{x} \in \mathbb{R}^d} f(\mathbf{x}) := -\log(\|\mathbf{x} - \mathbf{m}_1\|^2 + 10^{-5}) - \log(\|\mathbf{x} - \mathbf{m}_2\|^2 + 10^{-2}), \quad (7)$$

the global maximum point $\mathbf{m}_1 \in \mathbb{R}^d$ has all its entries equal to -0.5 , and the local maximum point $\mathbf{m}_2 \in \mathbb{R}^d$ has all its entries equal to 0.5 . The graph of its 2D-version is plotted in Figure 2.

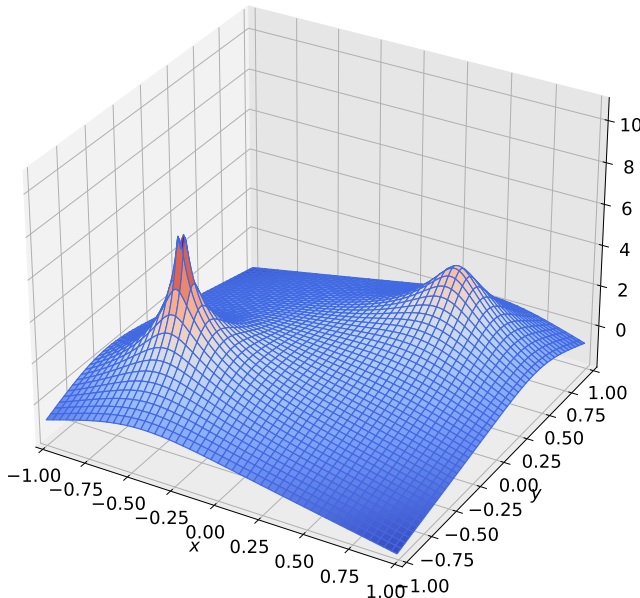


Figure 2: $f(\mathbf{x}) = -\log(\|\mathbf{x} - \mathbf{m}_1\|^2 + 10^{-5}) - \log(\|\mathbf{x} - \mathbf{m}_2\|^2 + 10^{-2})$

With each value of N , both the PGS and EGS are performed to solve this problem. The N -candidate set is $\{10, 20, \dots, 65\}$ for PGS and $\{1.0, 1.5, 2.0, \dots, 4.5\}$ for EGS. For each N value, we do 100 trials to stabilize the result. In each trial, the initial solution candidate $\boldsymbol{\mu}_0$ is uniformly sampled from $C := \{\mathbf{x} \in \mathbb{R}^d | x_i \in [-1.0, 1.0], i \in \{1, 2, \dots, d\}\}$, where x_i represents the i^{th} entry of \mathbf{x} . We set the initial learning rate as 0.1, the scaling parameter σ as 0.5, and the total number of solution updates as 1000. The objective for Power-GS is modified to be $f_1(\mathbf{x}) := f(\mathbf{x}) + 10$ to ensure that the PGS agent will not encounter negative fitness values during the 1000 updates.

We perform the experiments in two settings, one is two-dimensional ($d = 2$) and the other is five-dimensional ($d = 5$). The results, plotted in Figure 3, show that, as N increases, the distance between the produced solution $\boldsymbol{\mu}^*$ and the global maximum point \mathbf{x}^* approaches zero (see the decreasing MSE curve in the plot), which is consistent with Theorem 1 and the idea that $F(\boldsymbol{\mu})$'s maximum $\boldsymbol{\mu}^*$ approaches the global maximum point \mathbf{x}^* of f as we put more weight on $f(\mathbf{x}^*)$

5.2 Performance on Benchmark Objective Functions

In this subsection, we test the performance of PGS and EGS on solving (1), with the objective f being either of the two popular benchmark objective functions, the Ackley

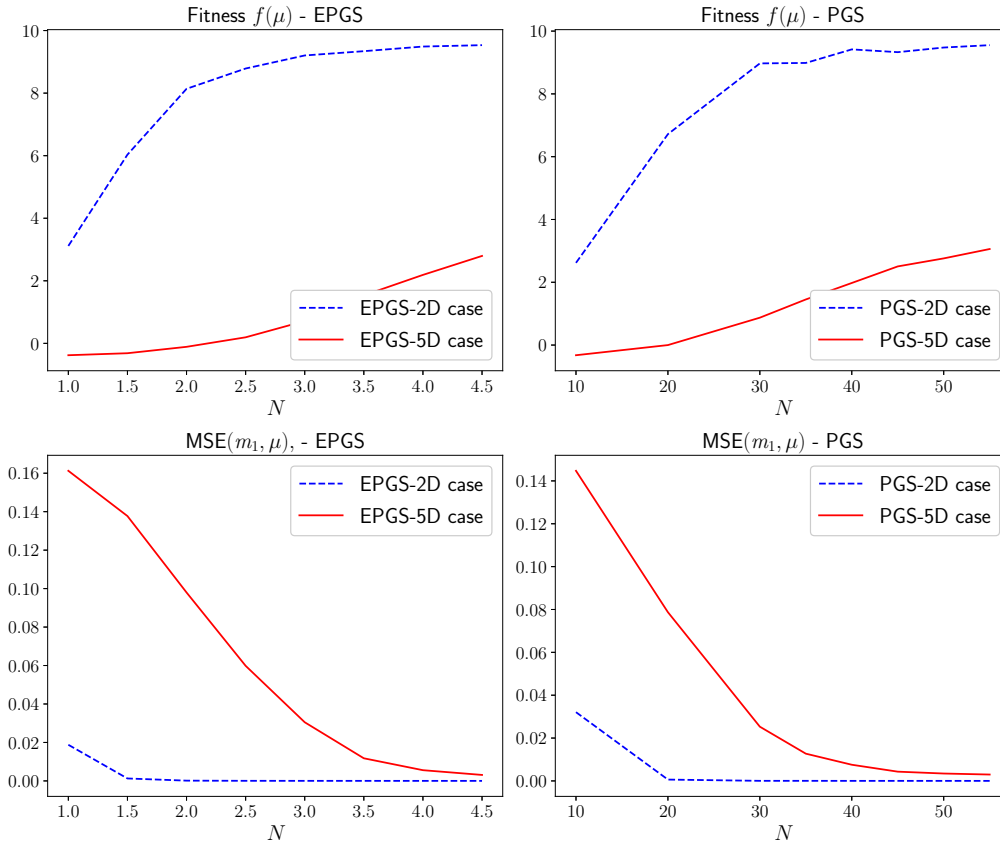


Figure 3: Effects of Increasing N . For each N , we perform the algorithm 100 times and obtain $\{\mu_k\}_{k=1}^{100}$. The average fitness $\sum_{k=1}^{100} f(\mu_k)/100$ and $\sum_{k=1}^{100} MSE(m_1, \mu_k)/100$ are plotted, where $MSE(m_1, \mu_k) := \sum_{i=1}^d (\mu_{ki} + 0.5)^2/d$, $\sigma = 1.0$, and f is defined in 7. Note that $x^* = m_1$ has all its entries equal to -0.5 .

and the Rosenbrock (max-version). The performances of other popular global algorithms (max-version) are also reported for comparison, including

- a standard homotopy method STD-Homotopy (see our appendix for details);
- two zeroth-order single-loop Gaussian homotopy algorithms (deterministic version⁷), ZO-SLGHd and ZO-SLGHr ([10, Algorithm 3]);
- the gradient-ascent version of the zeroth-order algorithm of ZO-SGD ([5, Equation (1)] and [8, Section 2.1]) and ZO-AdaMM([5, Algorithm 1])⁸, which were also used for comparisons in [10];
- as well as the evolutionary algorithm of (5) particle swarm optimization (PSO, e.g., [14, Section 3.1.5] and [15]).

The details on STD-Homotopy and ZO-SGD, as well as the selected hyper-parameter values of all algorithms, can be found in our appendix. More details can be found in our codes at <http://github.com/chen-research/GS-PowerTransform>.

⁷A deterministic version of SLGH is for solving the optimization problem of $\max_x f(x)$, with f being a deterministic function.

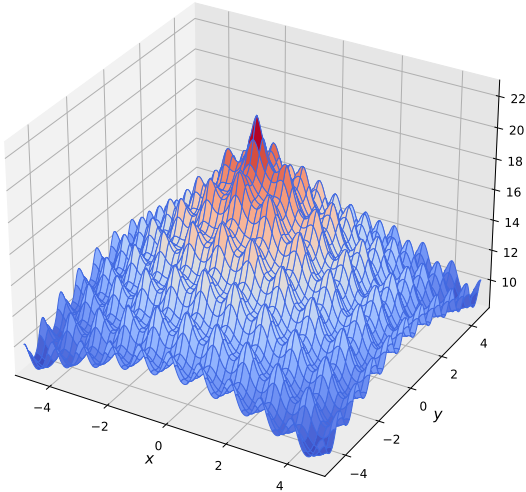
⁸ZO-SGD and ZO-AdaMM were originally designed to solves (2). We take their solutions to (2) as solutions to (1), and treat the scaling parameter in (2) as a hyper-parameter.

5.2.1 Ackley

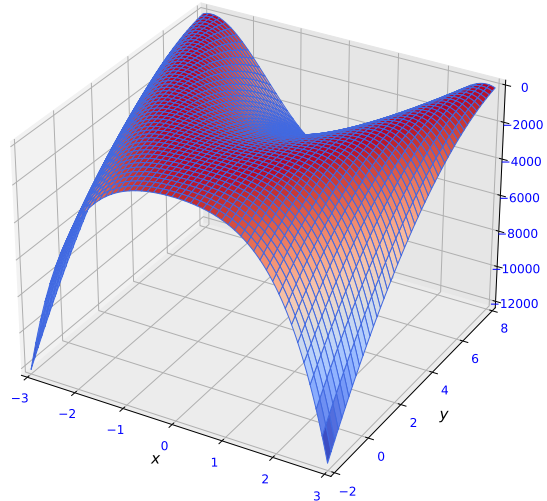
The Ackley objective function features with a numerous number of local optimums and a single global optimum. We solve the max-version of the corresponding problem, which is

$$\max_{(x,y) \in \mathbb{R}^2} f(x, y) := 20e^{-0.2\sqrt{0.5(x^2+y^2)}} + e^{0.5(\cos(2\pi x) + \cos(2\pi y))}.$$

The graph of this function is plotted in Figure 4(a). From both the functional form and the graph, it is not difficult to see that $f(x, y)$ attains its maximum at $(0, 0)$.



(a) Ackley Function (Max-Version)



(b) Rosenbrock Function (Max-Version).

Figure 4: Graph of objective functions.

The solutions and their fitness values found by each of the compared algorithms are reported in Table 1. From which we see that all of these algorithms are able to avoid the local maximum points and achieve the global maximum point.

5.2.2 Rosenbrock

The Rosenbrock objective is known to be difficult to optimize, since its global optimum point $\mathbf{x}^* = (1.0, 1.0)$ is surrounded by a flat curved plane (see Figure). Specifically, the problem to be solved is $\max_{(x,y) \in \mathbb{R}^2} f(x, y)$, where

$$f(x, y) = -100(y - x^2)^2 - (1 - x)^2.$$

We use PGS, EPGS, and other algorithms to solve $\max_{\mathbf{x}} f(\mathbf{x})$. Their performances are recorded in Table 2, which shows that EPGS, STD-Homotopy, and PSO are superior than other algorithms on this task, since they are able to locate the true solution of $(1,1)$.

5.2.3 Conclusions on Algorithm Performances for Benchmark Objectives

For Ackley, all the algorithms are able to locate the true solution of $(1,1)$, except PSO when the initial population is concentrated near the initial start of $\boldsymbol{\mu}_0$, which indicates that the performance of PSO depends more on the initial guess than other methods. For Rosenbrock, EPGS outperforms other algorithms except PSO (which is quite different since it does not apply smoothing).

Table 1: Performances on Maximizing Ackley. The limit of the number of iterations is set as 200, and 100 samples are used for each solution update. The hyper-parameters are selected by trials. For each set of hyper-parameter candidates, we perform 100 experiments and *take the average* to stabilize the results (all the reported numbers are averages). The initial solution value for each experiment is drawn from a multivariate Gaussian with mean $\boldsymbol{\mu}_0$ and covariance $0.01I_2$, where $\boldsymbol{\mu}_0 := [5.0, 5.0]$, except for PSO2 (for which $\text{cov} = 2I_2$). In the table, “Iterations Taken” refers to the number of iterations taken to reach the best found solution. All numbers are rounded to keep at most 3 decimal places. The global maximum point of the Ackley function is (0,0).

	Iterations Taken	Best Solution Found ($\boldsymbol{\mu}^*$)	$f(\boldsymbol{\mu}^*)$
EPGS ($N = 1$)	146.	(−0.001, −0.001)	22.682
PGS ($N = 20$)	141	(0.001, 0.002)	22.678
STD-Homotopy	194	(0.945, 0.901)	17.627
ZO-SLGHD	123	(−0.003, −0.001).	22.61
ZO-SLGHR	131	(0.001, −0.002).	22.621
ZO-AdaMM	158	(0.005, 0.001).	22.613
ZO-SGD	174	(0.005, 0.007).	22.596
PSO1	174	(4.425, 4.465).	10.974
PSO2	195	(0.0, 0.05).	22.617

Table 2: Performances on Maximizing Rosenbrock. The limit of the number of iterations is set as 1000, and 100 samples are used for each solution update. The hyper-parameters are selected by trials. For each set of hyper-parameter candidates, we perform 100 experiments and *take the average* to stabilize the results (all the reported numbers are averages). The initial solution value for each experiment is drawn from a multivariate Gaussian with mean $\boldsymbol{\mu}_0$ and covariance $0.01I_2$, where $\boldsymbol{\mu}_0 := [-3.0, 2.0]$. In the table, “Iterations Taken” refers to the number of iterations taken to reach the best found solution. For PGS, the Rosenbrock is added by 20,000 to ensure the search agent only encounter positive values. All numbers are rounded to keep at most 3 decimal places. The global maximum point of the Rosenbrock function is (1,1).

	Iterations Taken	Best Solution Found ($\boldsymbol{\mu}^*$)	$f(\boldsymbol{\mu}^*)$
EPGS ($N = 1$)	456.	(0.994, 1.002)	-0.18
PGS ($N = 1$)	513	(0.773, 1.025)	-22.8408
STD-Homotopy	624	(0.903, 0.885)	-2.401
ZO-SLGHD	471	(−0.447, 1.991).	-137.016
ZO-SLGHR	148	(0.105, 0.938).	-88.477
ZO-AdaMM	1736	(0.004, 0.618).	-39.206
ZO-SGD	45	(0.272, 1.173).	-121.14
PSO	374	(1.0, 1.0).	0.0

5.3 Performance on the Black-box Targeted Adversarial Attack

Let \mathcal{C} be an black-box⁹ image classifier. The targeted adversarial attack on \mathcal{C} refers to the task of modifying the pixels of a given image \mathbf{a} so that $\mathcal{C}(\mathbf{a} + \mathbf{x})$ is equal to a pre-specified

⁹A black-box classifier refers to a classification model whose parameters are not accessible.

target label \mathcal{T} . We perform attacks in the most difficult case - the target label \mathcal{T} is pre-selected to be the one with the smallest predicted probability. Another goal of this task is to minimize the perturbation size $\|\mathbf{x}\|$. Hence, we set the loss as

$$L(\mathbf{x}) := \max(\max_{i \neq \mathcal{T}} \mathcal{C}(\mathbf{a} + \mathbf{x})_i - \mathcal{C}(\mathbf{a} + \mathbf{x})_{\mathcal{T}}, \kappa) + \lambda \|\mathbf{x}\|,$$

where $\mathcal{C}(\mathbf{a} + \mathbf{x})_i$ denotes the predicted logit (i.e., log probability) for the i^{th} class, κ is a hyper-parameter that controls the certainty level of the attack, λ is a regularization coefficient (we set $\lambda = 1$ in our experiments), $\mathcal{T} := \arg \min_i \mathcal{C}(\mathbf{a})_i$, and $\|\mathbf{x}\|$ denotes the L_1 norm of \mathbf{x} (i.e., the square root of the sum of squares of entries in \mathbf{x}). This loss function resembles the popular one designed in [3].

With EPGS and other compared algorithms, we perform adversarial attacks on 100 randomly selected images from each of two image datasets, the set of MNIST figures ([12]) and the CIFAR-10 set ([11]). Specifically, the goal is to solve:

$$\max_{\mathbf{x} \in \mathbb{R}^d} f(\mathbf{x}) := -L(\mathbf{x}),$$

where d is the total number of pixels in each image. For Figure-MNIST images, $d = 28 \times 28$, and for CIFAR-10 images, $d = 32 \times 32 \times 3$. We call f as the fitness function.

The classifier is a robust convolutional neural network (CNN) trained using the technique of defensive distillation¹⁰. The distillation temperature is set at 100, which leads to a high level of robustness ([3]). In the Figure-MNIST attacks, our trained classifier \mathcal{C} has a classification accuracy of 97.4% on the testing images. In the CIFAR-10 attacks, the trained \mathcal{C} has a test accuracy of 87.0%.

The hyper-parameters of all the tested algorithms are selected by trials and can be found in Appendix 7.4. For ZO-SLGHD, ZO-SLGHr, and ZO-AdaMM, the hyper-parameters selected in [10, Appendix E.1] are included in our candidate set, since they performed similar tasks.

We choose EPGS over PGS for this task since the fitness function $f(\mathbf{x})$ can be negative, which makes EPGS more convenient to apply. (But note that we can modify $f(\mathbf{x})$ by adding a large positive constant to facilitate PGS).

5.3.1 MNIST

For each image \mathbf{a}_m that is randomly drawn from the testing dataset, where $m \in \{1, 2, \dots, 100\}$, and each algorithm, we perform an attack (i.e., experiment) of T_{total} iterations. Let $\{\boldsymbol{\mu}_{m,t}\}_{t=0}^{T_{total}-1}$ denote all the perturbations (solutions) produced in these T_{total} iterations. We say that a perturbation $\boldsymbol{\mu}$ is successful if the predicted log probability of the target label is at least $\kappa = 0.01$ greater than that of other classes (i.e., $\mathcal{C}(\mathbf{a} + \boldsymbol{\mu})_{\mathcal{T}} - \max_{i \neq \mathcal{T}} \mathcal{C}(\mathbf{a} + \boldsymbol{\mu})_i > \kappa$). We say that an attack is successful if the produced $\{\boldsymbol{\mu}_{m,t}\}_{t=0}^{T_{total}-1}$ contains at least one successful perturbation. If the attack is successful, let $\boldsymbol{\mu}_m^*$ denote the successful perturbation with the largest R^2 -value among $\{\boldsymbol{\mu}_{m,t}\}_{t=0}^{T_{total}-1}$, and let T_m denote the number of iterations taken by the algorithm to produce $\boldsymbol{\mu}_m^*$. Here, the R^2 -value of $\boldsymbol{\mu}$ refers to the R^2 statistic between \mathbf{a} and the perturbed image $\mathbf{a} + \boldsymbol{\mu}$, which is computed as $\frac{\sum_{i=1}^d (a_i - \bar{a})^2}{\sum_{i=1}^d \mu_i^2}$. In this formula, a_i and μ_i ranges over all the pixels (entries) of \mathbf{a} and $\boldsymbol{\mu}$.

With the above notations, we construct three measures on the performances of an algorithm. One is the success rate, which refers to the ratio of successful image attacks out

¹⁰We borrow the code by [3] for training the classifier from https://github.com/carlini/nn_robust_attacks, which applies TensorFlow ([1]) for model training. We changed the layer structure in the neural network to either increase accuracy or to decrease computation complexity.

of the total number of attacks (100). The second measure is the average R^2 , which equals $\bar{R}^2 := \sum_{m \in \mathbb{S}} R^2(\mathbf{a}_m, \mathbf{a}_m + \boldsymbol{\mu}_m^*) / |\mathbb{S}|$, where \mathbb{S} denotes the set of indices of the successful attacks. The last measure is the average \bar{T} of $\{T_m\}_{m \in \mathbb{S}}$.

The results are reported in Table 3, from which we see that EPGS has a significantly higher \bar{R}^2 -score (i.e., 85%) than other algorithms, indicating that the perturbed image is closest to the original one. Also, the average number of iterations taken by EPGS to reach the optimal perturbation is 438, which is among the two fastest algorithms.

Table 3: Targeted Adversarial Attack on 100 MNIST hand-written figures (per-image). For each image attack, the initial perturbation is set as $\boldsymbol{\mu}_0 := \mathbf{0}$. For each image, 1,500 iterations of are performed by each algorithm. The success rate is the portion of successful attacks out of the 100 attacks. \bar{R}^2 is the average of $\{R^2(\mathbf{a}_m, \mathbf{a}_m + \boldsymbol{\mu}_m^*)\}_{m \in \mathbb{S}}$, where \mathbf{a}_m denotes the m^{th} original image and $\boldsymbol{\mu}_m^*$ denotes the optimal perturbation found in the m^{th} image attack, and \mathbb{S} denotes the set of indices of the successful attacks. \bar{T} denotes the average number of iterations taken to the optimal perturbation. The numbers in the parentheses are sample standard deviations.

	Success Rate	\bar{R}^2	\bar{T}
EPGS ($N = .02$)	100%.	.85 (.05)	438 (120)
ZO-SLGHD	100%	.54 (.14)	1491 (43)
ZO-SLGHr	100%	.36 (.26)	522 (688)
ZO-SGD	100%	-3.30 (1.67)	2997 (15)
ZO-AdaMM	100%	0.24 (.26)	50 (25)
STD-Homotopy	86%	-.05 (.36)	559 (303)

5.3.2 CIFAR-10

We perform per-image targeted adversarial attacks on 100 randomly drawn images from the testing set. The experiments are performed in the same way as that for Figure-MNIST, and their results are reported in Table 4. These results are in general better than those in the Figure-MNIST attacks, which we believe is because of the lower accuracy of the CIFAR-10 CNN.

The results show that EPGS produces a success rate of 100% and scores the second with respect to \bar{R}^2 . Specifically, the \bar{R}^2 -value of 98% indicates that the perturbed image produced by EPGS is very close to the original image ($\bar{R}^2 = 100\%$ implies that the two are identical), which is consistent with our goal that the perturbation size $\|\boldsymbol{\mu}_*\|$ should be small.

In this experiment, among the algorithms that attain a 100% success rate, with an \bar{R}^2 score of 99%, ZO-SLGHD outperforms other algorithms. EPGS’s performance of $\bar{R}^2 = 98\%$ is very close to that of ZO-SLGHD.

5.4 Summary on Experiment Results

The experiments show that PGS and EPGS ranked among the tops in all the tasks they performed. In the tasks of Ackley and Rosenbrock (Table 2 and 3), EPGS has the highest fitness value $f(\boldsymbol{\mu}^*)$ than other algorithms that also apply smoothing techniques. For Figure-MNIST attacks (Table 3), EPGS has a significantly higher \bar{R}^2 score. For CIFAR-10 attacks (Table 4), EPGS’s \bar{R}^2 score is very close to that of the best (ZO-SLGHD). In sum,

EPGS outperforms other algorithms that also apply smoothing techniques in most of our experiments.

Table 4: Targeted Adversarial Attack on 100 CIFAR-10 images (per-image). For each image, 1,500 iterations of are performed by each algorithm. The initial perturbation is set as $\boldsymbol{\mu}_0 := \mathbf{0}$. In the table, “Succ. Rate”, \bar{R}^2 and \bar{T} are defined in the same way as in Table 3. All numbers are rounded to keep 3 decimal places.

	Success Rate	\bar{R}^2	\bar{T}
EPGS ($N = 0.03$)	100%.	.98 (.02)	686 (277)
ZO-SLGHd	100%	.99 (.01)	1288 (429)
ZO-SLGHr	100%	.98 (.02)	402 (307)
ZO-SGD	69%	.99 (.00)	680 (370)
ZO-AdaMM	100%	.66 (.27)	64(149)
STD-Homotopy	69%	.86 (.13)	479 (349)

6 Conclusion

In this paper, we propose a novel smoothing method, GSPTO, for solving the global optimization problem of (1), which is featured with putting more weight on the objective’s global optimum through power transformations. Both our theoretical analysis and numerical experiments show that GSPTO outperforms other optimization algorithms that also apply smoothing techniques. This method provides a foundation for future studies to explore more efficient ways to increase the gap between $f(\mathbf{x}^*)$ and other values before smoothing.

References

- [1] M. Abadi, A. Agarwal, P. Barham, E. Brevdo, Z. Chen, C. Citro, G. S. Corrado, A. Davis, J. Dean, M. Devin, S. Ghemawat, I. Goodfellow, A. H., G. Irving, M. Isard, Y. Jia, R. Jozefowicz, L. Kaiser, M. Kudlur, J. Levenberg, D. Mane, R. Monga, S. Moore, D. Murray, C. Olah, M. Schuster, J. Shlens, B. Steiner, I. Sutskever, K. Talwar, P. Tucker, V. Vanhoucke, V. Vasudevan, F. Viegas, O. Vinyals, P. Warden, M. Wattenberg, M. Wicke, Y. Yu, and X. Zheng. Tensorflow: Large-scale machine learning on heterogeneous distributed systems, 2015.
- [2] A. Blake and A. Zisserman. *Visual Reconstruction*. MIT press, 1987.
- [3] N. Carlini and D. Wagner. Towards evaluating the robustness of neural networks. In *2017 IEEE Symposium on Security and Privacy (SP)*, pages 39–57, 2017.
- [4] J. Chen, Z. Guo, H. Li, and C. P. Chen. Regularizing scale-adaptive central moment sharpness for neural networks. *IEEE Transactions on Neural Networks and Learning Systems*, 35(5), 2024.
- [5] X. Chen, S. Liu, K. Xu, X. Li, X. Lin, M. Hong, and D. Cox. Zo-adamm: Zeroth-order adaptive momentum method for black-box optimization. *Advances in neural information processing systems*, 32, 2019.

- [6] K. Dvijotham, M. Fazel, and E. Todorov. Universal convexification via risk-aversion. In *Proceedings of the Thirtieth Conference on Uncertainty in Artificial Intelligence*, 2014.
- [7] K. Gao and O. Sener. Generalizing Gaussian smoothing for random search. In *Proceedings of the 39th International Conference on Machine Learning*, volume 162, pages 7077–7101. PMLR, 2022.
- [8] S. Ghadimi and G. Lan. Stochastic first-and zeroth-order methods for nonconvex stochastic programming. *SIAM journal on optimization*, 23(4):2341–2368, 2013.
- [9] E. Hazan, K. Y. Levy, and S. Shalev-Shwartz. On graduated optimization for stochastic non-convex problems. In *Proceedings of The 33rd International Conference on Machine Learning*, volume 48, pages 1833–1841, 2016.
- [10] H. Iwakiri, Y. Wang, S. Ito, and A. Takeda. Single loop gaussian homotopy method for non-convex optimization. In *Advances in Neural Information Processing Systems*, volume 35, pages 7065–7076. Curran Associates, Inc., 2022.
- [11] A. Krizhevsky and G. Hinton. Learning multiple layers of features from tiny images. Technical Report TR-2009, University of Toronto, 2009.
- [12] Y. LeCun, L. Bottou, Y. Bengio, and P. Haffner. Gradient-based learning applied to document recognition. *Proceedings of the IEEE*, 86(11):2278–2324, 1998.
- [13] X. Lin, Z. Yang, X. Zhang, and Q. Zhang. Continuation path learning for homotopy optimization. In *Proceedings of the 40th International Conference on Machine Learning*, volume 202, pages 21288–21311. PMLR, 2023.
- [14] M. Locatelli and F. Schoen. *Global Optimization: Theory, Algorithms, and Applications*. SIAM, Philadelphia, PA, 2013.
- [15] L. J. V. Miranda. PySwarms, a research-toolkit for particle swarm optimization in python. *Journal of Open Source Software*, 3, 2018.
- [16] H. Mobahi and J. F. III. A theoretical analysis of optimization by gaussian continuation. In *Proceedings of the AAAI Conference on Artificial Intelligence*, volume 29, pages 1205–1211, 2015.
- [17] H. Mobahi and Y. Ma. Gaussian smoothing and asymptotic convexity. Technical report, University of Illinois at Urbana-Champaign, 2012.
- [18] Y. Nesterov and V. Spokoiny. Random gradient-free minimization of convex functions. *Foundations of Computational Mathematics*, 17(2):527–566, 2017.
- [19] V. Roulet, M. Fazel, S. Srinivasa, and Z. Harchaoui. On the convergence of the iterative linear exponential quadratic gaussian algorithm to stationary points. In *2020 American Control Conference (ACC)*, pages 132–137. IEEE, 2020.
- [20] A. Starnes and C. Webster. Improved performance of stochastic gradients with gaussian smoothing, 2024.
- [21] L. Xiao and T. Zhang. A proximal-gradient homotopy method for the l1-regularized least-squares problem. In *Proceedings of the 29th International Conference on Machine Learning (ICML-12)*, pages 839–846, 2012.

- [22] Y. Xu, Y. Yan, Q. Lin, and T. Yang. Homotopy smoothing for non-smooth problems with lower complexity than $o(1/\epsilon)$. In *Advances in Neural Information Processing Systems*, volume 29. Curran Associates, Inc., 2016.

7 Appendix

7.1 Proof to Theorem 1 for EPGs

Proof. Recall that for EPGs, $f_N(\mathbf{x}_k) := \begin{cases} e^{Nf(\mathbf{x}_k)}, & \mathbf{x} \in \mathcal{S}; \\ 0, & \text{otherwise.} \end{cases}$ For any given $\delta > 0$, define $V_\delta := \sup_{\mathbf{x}: \|\mathbf{x} - \mathbf{x}^*\| \geq \delta} f(\mathbf{x})$ and $D_\delta := (V_\delta + f(\mathbf{x}^*))/2$. Using this symbol, we re-write $F_N(\boldsymbol{\mu}, \sigma)$ as

$$F_N(\boldsymbol{\mu}, \sigma) = e^{D_\delta N} G_N(\boldsymbol{\mu}, \sigma) = e^{D_\delta N} (H_N(\boldsymbol{\mu}, \sigma) + R_N(\boldsymbol{\mu}, \sigma)), \quad (8)$$

where

$$\begin{aligned} G_N(\boldsymbol{\mu}, \sigma) &:= (\sqrt{2\pi}\sigma)^{-d} \int_{\mathbf{x} \in \mathbb{R}^d} e^{-ND_\delta} f_N(\mathbf{x}) e^{-\frac{\|\mathbf{x} - \boldsymbol{\mu}\|^2}{2\sigma^2}} d\mathbf{x}, \\ H_N(\boldsymbol{\mu}, \sigma) &:= (\sqrt{2\pi}\sigma)^{-d} \int_{\mathbf{x} \in B(\mathbf{x}^*; \delta)} e^{-ND_\delta} f_N(\mathbf{x}) e^{-\frac{\|\mathbf{x} - \boldsymbol{\mu}\|^2}{2\sigma^2}} d\mathbf{x}, \\ R_N(\boldsymbol{\mu}, \sigma) &:= (\sqrt{2\pi}\sigma)^{-d} \int_{\mathbf{x} \notin B(\mathbf{x}^*; \delta)} e^{-ND_\delta} f_N(\mathbf{x}) e^{-\frac{\|\mathbf{x} - \boldsymbol{\mu}\|^2}{2\sigma^2}} d\mathbf{x}, \end{aligned}$$

where $B(\mathbf{x}^*; \delta) := \{\mathbf{x} \in \mathbb{R}^d : \|\mathbf{x} - \mathbf{x}^*\| < \delta\}$.

We derive an upper bound for $\left| \frac{\partial R_N(\boldsymbol{\mu}, \sigma)}{\partial \mu_i} \right|$. For any $\boldsymbol{\mu} \in \mathbb{R}^d$,

$$\begin{aligned} \left| \frac{\partial R_N(\boldsymbol{\mu}, \sigma)}{\partial \mu_i} \right| &\leq \frac{1}{(\sqrt{2\pi})^d \sigma^{d+2}} \int_{\mathbf{x} \notin B(\mathbf{x}^*; \delta)} |x_i - \mu_i| e^{-\frac{\|\mathbf{x} - \boldsymbol{\mu}\|^2}{2\sigma^2}} e^{-ND_\delta} f_N(\mathbf{x}) d\mathbf{x} \\ &\leq \frac{1}{(\sqrt{2\pi})^d \sigma^{d+2}} \int_{\mathbf{x} \notin B(\mathbf{x}^*; \delta)} |x_i - \mu_i| e^{-\frac{\|\mathbf{x} - \boldsymbol{\mu}\|^2}{2\sigma^2}} e^{N(f(\mathbf{x}) - D_\delta)} d\mathbf{x} \\ &\leq \frac{1}{(\sqrt{2\pi})^d \sigma^{d+2}} \int_{\mathbf{x} \notin B(\mathbf{x}^*; \delta)} |x_i - \mu_i| e^{-\frac{\|\mathbf{x} - \boldsymbol{\mu}\|^2}{2\sigma^2}} e^{N(V_\delta - D_\delta)} d\mathbf{x} \\ &\leq \frac{e^{N(V_\delta - D_\delta)}}{(\sqrt{2\pi})^d \sigma^{d+2}} \int_{\mathbf{x} \in \mathbb{R}^d} |x_i - \mu_i| e^{-\frac{\|\mathbf{x} - \boldsymbol{\mu}\|^2}{2\sigma^2}} d\mathbf{x} \\ &\leq e^{N(V_\delta - D_\delta)} \left(\prod_{j \neq i} \frac{1}{\sqrt{2\pi}\sigma} \int_{x_j \in \mathbb{R}} e^{-\frac{(x_j - \mu_j)^2}{2\sigma^2}} dx_j \right) \\ &\quad \cdot \frac{1}{\sqrt{2\pi}\sigma^3} \int_{x_i \in \mathbb{R}} |x_i - \mu_i| e^{-\frac{(x_i - \mu_i)^2}{2\sigma^2}} dx_i \quad (9) \\ &= e^{N(V_\delta - D_\delta)} \frac{1}{\sqrt{2\pi}\sigma^3} \int_{y \in \mathbb{R}} \sqrt{2}\sigma |y| e^{-y^2} d(\sqrt{2}\sigma y), \quad y := \frac{x_i - \mu_i}{\sqrt{2}\sigma}, \\ &= e^{N(V_\delta - D_\delta)} \frac{\sqrt{2}}{\sqrt{\pi}\sigma} \cdot 2 \int_0^\infty y e^{-y^2} dy, \quad y := \frac{x_i - \mu_i}{\sqrt{\pi}\sigma}, \\ &= e^{N(V_\delta - D_\delta)} \frac{\sqrt{2}}{\sqrt{\pi}\sigma} \cdot \int_0^\infty e^{-y^2} dy^2, \\ &= e^{N(V_\delta - D_\delta)} \frac{\sqrt{2}}{\sqrt{\pi}\sigma} \cdot \int_0^\infty e^{-z} dz, \\ &= \frac{\sqrt{2} e^{N(V_\delta - D_\delta)}}{\sqrt{\pi}\sigma} \end{aligned}$$

where the third line is because $\|\mathbf{x} - \mathbf{x}^*\| \geq \delta \Rightarrow f(\mathbf{x}) \leq V_\delta$, and the fifth line is by the separability of a multivariate integral.

Since f is continuous, for $\epsilon_\delta := f(\mathbf{x}^*) - D_\delta > 0$ (because $V_\delta < f(\mathbf{x}^*)$), there exists $\delta' \in (0, \delta)$ such that whenever $\|\mathbf{x} - \mathbf{x}^*\| \leq \delta'$,

$$f(\mathbf{x}) \geq f(\mathbf{x}^*) - \epsilon_\delta = D_\delta > V_\delta. \quad (10)$$

Using this result, we derive a lower bound for $\left| \frac{\partial H_N(\boldsymbol{\mu}, \sigma)}{\partial \mu_i} \right|$ when $\|\boldsymbol{\mu}\| \leq M$ and $|\mu_i - x_i^*| > \delta$.

$$\begin{aligned} \left| \frac{\partial H_N(\boldsymbol{\mu}, \sigma)}{\partial \mu_i} \right| &= \frac{1}{(\sqrt{2\pi})^d \sigma^{d+2}} \int_{\mathbf{x} \in B(\mathbf{x}^*; \delta)} |x_i - \mu_i| e^{-ND_\delta} f_N(\mathbf{x}) e^{-\frac{\|\mathbf{x} - \boldsymbol{\mu}\|^2}{2\sigma^2}} d\mathbf{x} \\ &= \frac{1}{(\sqrt{2\pi})^d \sigma^{d+2}} \int_{\mathbf{x} \in B(\mathbf{x}^*; \delta)} |x_i - \mu_i| e^{-\frac{\|\mathbf{x} - \boldsymbol{\mu}\|^2}{2\sigma^2}} e^{N(f(\mathbf{x}) - D_\delta)} d\mathbf{x}, \text{ since } B(\mathbf{x}^*; \delta) \subset \mathcal{S}, \\ &\geq \frac{1}{(\sqrt{2\pi})^d \sigma^{d+2}} \int_{\mathbf{x} \in B(\mathbf{x}^*; \delta')} |x_i - \mu_i| e^{-\frac{\|\mathbf{x} - \boldsymbol{\mu}\|^2}{2\sigma^2}} e^{N(f(\mathbf{x}) - D_\delta)} d\mathbf{x} \\ &\stackrel{\text{by (10)}}{\geq} \frac{1}{(\sqrt{2\pi})^d \sigma^{d+2}} \int_{\mathbf{x} \in B(\mathbf{x}^*; \delta')} (\delta - \delta') e^{-\frac{\|\mathbf{x} - \boldsymbol{\mu}\|^2}{2\sigma^2}} d\mathbf{x} \\ &\geq \frac{1}{(\sqrt{2\pi})^d \sigma^{d+2}} \int_{\mathbf{x} \in B(\mathbf{x}^*; \delta')} (\delta - \delta') e^{-\frac{M^2}{\sigma^2}} e^{-\frac{\|\mathbf{x}\|^2}{\sigma^2}} d\mathbf{x}, \quad \|\mathbf{x} - \boldsymbol{\mu}\|^2 \leq 2(\|\mathbf{x}\|^2 + \|\boldsymbol{\mu}\|^2), \\ &\geq (\delta - \delta') e^{-\frac{M^2}{\sigma^2}} V(\delta', d, \sigma) \end{aligned} \quad (11)$$

where the first equality is implied by the fact that $x_i - \mu_i$ does not change sign as \mathbf{x} travels in $B(\mathbf{x}^*; \delta)$ (this fact is because of $|\mu_i - x_i^*| > \delta$), and

$$V(\delta', d, \sigma) = \frac{1}{(\sqrt{2\pi})^d \sigma^{d+2}} \int_{\mathbf{x} \in B(\mathbf{x}^*; \delta')} e^{-\frac{\|\mathbf{x}\|^2}{\sigma^2}} d\mathbf{x}.$$

The positive number $N_{\delta, \sigma, M}$ is constructed by solving the following inequality for N , which involves the two bounds in (9) and (11).

$$\frac{\sqrt{2} e^{N(V_\delta - D_\delta)}}{\sqrt{\pi} \sigma} < (\delta - \delta') e^{-\frac{M^2}{\sigma^2}} V(\delta', d, \sigma).$$

The solution of this inequality is

$$N > \frac{\ln \left(\frac{\sqrt{\pi}}{\sqrt{2}} (\delta - \delta') e^{-\frac{M^2}{\sigma^2}} V(\delta', d, \sigma) \right)}{V_\delta - D_\delta},$$

where $V_\delta - D_\delta < 0$ and the numerator is negative for sufficiently large $M > 0$. Therefore, whenever

$$N > N_{\delta, \sigma, M} := \max \left\{ 0, \frac{\ln \left(\frac{\sqrt{\pi}}{\sqrt{2}} (\delta - \delta') e^{-\frac{M^2}{\sigma^2}} V(\delta', d, \sigma) \right)}{V_\delta - D_\delta} \right\},$$

we have

$$\left| \frac{\partial R_N(\boldsymbol{\mu}, \sigma)}{\partial \mu_i} \right| < \frac{\sqrt{2} e^{N(V_\delta - D_\delta)}}{\sqrt{\pi} \sigma} < (\delta - \delta') e^{-\frac{M^2}{\sigma^2}} V(\delta', d, \sigma) < \left| \frac{\partial H_N(\boldsymbol{\mu}, \sigma)}{\partial \mu_i} \right|. \quad (12)$$

When $N > N_{\delta, \sigma, M}$, $\|\boldsymbol{\mu}\| \leq M$, and $\mu_i > x_i^* + \delta$,

$$\begin{aligned}
\frac{\partial G_N(\boldsymbol{\mu}, \sigma)}{\partial \mu_i} &= \frac{\partial H_N(\boldsymbol{\mu}, \sigma)}{\partial \mu_i} + \frac{\partial R_N(\boldsymbol{\mu}, \sigma)}{\partial \mu_i} \\
&= \frac{1}{(\sqrt{2\pi})^k \sigma^{k+2}} \int_{\mathbf{x} \in B(\mathbf{x}^*; \delta)} (x_i - \mu_i) e^{-\frac{\|\mathbf{x} - \boldsymbol{\mu}\|^2}{2\sigma^2}} e^{N(f(\mathbf{x}) - D_\delta)} d\mathbf{x} + \frac{\partial R_N(\boldsymbol{\mu}, \sigma)}{\partial \mu_i} \\
&= - \left| \frac{\partial H_N(\boldsymbol{\mu}, \sigma)}{\partial \mu_i} \right| + \frac{\partial R_N(\boldsymbol{\mu}, \sigma)}{\partial \mu_i} \\
&\stackrel{\text{by (12)}}{<} - \left| \frac{\partial R_N(\boldsymbol{\mu}, \sigma)}{\partial \mu_i} \right| + \left| \frac{\partial R_N(\boldsymbol{\mu}, \sigma)}{\partial \mu_i} \right| \\
&= 0,
\end{aligned} \tag{13}$$

where the third line is because the integrand of the first term is always negative in the integration region.

On the other hand, when $N > N_{\delta, \sigma, M}$, $\|\boldsymbol{\mu}\| \leq M$, and $\mu_i < x_i^* - \delta$,

$$\begin{aligned}
\frac{\partial G_N(\boldsymbol{\mu}, \sigma)}{\partial \mu_i} &= \frac{\partial H_N(\boldsymbol{\mu}, \sigma)}{\partial \mu_i} + \frac{\partial R_N(\boldsymbol{\mu}, \sigma)}{\partial \mu_i} \\
&= \left| \frac{\partial H_N(\boldsymbol{\mu}, \sigma)}{\partial \mu_i} \right| + \frac{\partial R_N(\boldsymbol{\mu}, \sigma)}{\partial \mu_i} \\
&\stackrel{\text{by (12)}}{>} \left| \frac{\partial R_N(\boldsymbol{\mu}, \sigma)}{\partial \mu_i} \right| - \left| \frac{\partial R_N(\boldsymbol{\mu}, \sigma)}{\partial \mu_i} \right| \\
&= 0.
\end{aligned} \tag{14}$$

Then, (13) and (14) imply the result in the theorem since $\frac{\partial G_N(\boldsymbol{\mu}, \sigma)}{\partial \mu_i}$ and $\frac{\partial F_N(\boldsymbol{\mu}, \sigma)}{\partial \mu_i}$ share the same sign (see Eq. (8)). \square

7.2 STD-Homotopy

STD-Homotopy is a standard homotopy algorithm for optimization. It has a double-loop mechanism. The inner loop updates the solution $\boldsymbol{\mu}_t$ with a fixed scaling parameter σ until no improvements of $f(\boldsymbol{\mu}_t)$ are made, and the outer loop decays σ iteratively. In this algorithm, the term $\widehat{\nabla F}(\boldsymbol{\mu}, \sigma)$ is an estimate of $\nabla_{\boldsymbol{\mu}} \mathbb{E}_{\mathbf{x} \sim \mathcal{N}(\boldsymbol{\mu}, \sigma I_d)}[f(\mathbf{x})] = \mathbb{E}_{\mathbf{x} \sim \mathcal{N}(\boldsymbol{\mu}, \sigma I_d)}[(\mathbf{x} - \boldsymbol{\mu}) f(\mathbf{x})]$, which is used to update $\boldsymbol{\mu}$.

7.3 ZO-SGD

The zeroth-order stochastic gradient ascent (ZO-SGD) is a max-version of [5, Equation (1)], whose gradient estimate method is from [18].

7.4 Hyper-parameters

For experiments on the benchmark test functions (Table 5 and 6), the set of hyper-parameter values with the smallest mean square error (averaged over the 100 experiments) between the true and estimated solutions are selected.

For the image attacks (Table 7 and 8), for each set of the hyper-parameter candidate values, we randomly choose 10 images to attack. The set with the highest average fitness value (average over the 10 image attacks) will be selected.

Algorithm 2: STD-Homotopy

Require: The maximum of iteration number $T_{total} > 0$, the initial scaling parameter $\sigma > 0$, the objective f , the initial value $\boldsymbol{\mu}_0$, the number K of sampled points for gradient approximation, the maximum number N_σ of times σ gets updated, the maximum T_μ of the number of times $\boldsymbol{\mu}$ gets updated for each value of σ , the tolerance number τ for no improvements of $f(\boldsymbol{\mu}_t)$ for any fixed σ , the decay factor $\gamma \in (0, 1)$, and the learning rate $\alpha_t > 0$.

Result: $\boldsymbol{\mu}_{t_1}$ - The approximated solution to (1).

$t_1 = 0, n_\sigma = 0$.

while $t_1 \leq T_{total}$ and $n_\sigma < N_\sigma$ **do**

$t = 0, I = True$.

while $t < T_\mu$ and $I == True$ and $t_1 \leq T_{total}$ **do**

 Independently and uniformly sample K points $\{\mathbf{v}_k\}_{k=1}^K$ from the uniform sphere in \mathbb{R}^d . Compute $\mathbf{x}_k := \boldsymbol{\mu}_t + \sigma \mathbf{v}_k$, for each k .

 Compute the gradient estimate $\widehat{\nabla F}(\boldsymbol{\mu}_t, \sigma) = \frac{1}{K} \sum_{k=1}^K (\mathbf{x}_k - \boldsymbol{\mu}_t) f(\mathbf{x}_k)$.

$\boldsymbol{\mu}_{t+1} = \boldsymbol{\mu}_t + \alpha_t \widehat{\nabla F}_N(\boldsymbol{\mu}_t, \sigma) / \|\widehat{\nabla F}_N(\boldsymbol{\mu}_t, \sigma)\|$.

if $\max\{f(\boldsymbol{\mu}_{t+1}), f(\boldsymbol{\mu}_t), \dots, f(\boldsymbol{\mu}_{t-\tau+1})\} \leq f(\boldsymbol{\mu}_{t-\tau})$ **then**

$I = False$.

end

$t_1 = t_1 + 1, t = t + 1$.

end

$\sigma = \gamma \sigma, n_\sigma = n_\sigma + 1$.

end

Return($\boldsymbol{\mu}_{t_1}$).

Algorithm 3: ZO-SGD

Require: The scaling parameter $\sigma > 0$, the objective f , the initial value $\boldsymbol{\mu}_0 \in \mathbb{R}^d$, the number K of sampled points for gradient approximation, the total number T of $\boldsymbol{\mu}$ -updates, and the learning rate schedule $\{\alpha_t\}_{t=1}^T$.

Result: $\boldsymbol{\mu}_T$ - The approximated solution to (1).

for t from 0 to $T-1$ **do**

 Independently and uniformly sample K points $\{\mathbf{v}_k\}_{k=1}^K$ from the uniform sphere in \mathbb{R}^d .

 Compute the gradient estimate

$$\widehat{\nabla F}(\boldsymbol{\mu}_t, \sigma) = \frac{1}{K} \sum_{k=1}^K \frac{(f(\boldsymbol{\mu}_t + \sigma \mathbf{v}_k) - f(\boldsymbol{\mu}_t)) \mathbf{v}_k}{\sigma}.$$

$\boldsymbol{\mu}_{t+1} = \boldsymbol{\mu}_t + \alpha_t \widehat{\nabla F}_N(\boldsymbol{\mu}_t, \sigma)$.

end

Return($\boldsymbol{\mu}_T$).

Table 5: Hyper-parameters for Optimizing Ackley. The candidate set for learning rates is $\mathcal{L} := \{.1, .001\}$. The candidate set for smoothing parameters is $\mathcal{S} := \{.1, 1.0, 2.0\}$. t_1 in ZO-SLGHd and ZO-SLGHr is the initial scaling parameter. μ in ZO-AdaMM is the scaling parameter. The set of candidate values that lead to the minimum mean square error between the true solution and the found solution will be selected.

	Selected Values	Candidates (μ^*)
EPGS	$\alpha_0 = .1, N = 1, \sigma = 1.0.$	$N \in \{1, 2, 3\}, \alpha_0 \in \mathcal{L}, \sigma \in \mathcal{S}.$
PGS	$\alpha_0 = .1, N = 20, \sigma = 1.0.$	$N \in \{5, 10, 20, 30\}, \alpha_0 \in \mathcal{L}, \sigma \in \mathcal{S}.$
STD-Homotopy	$\alpha = .1, \gamma = .8, \sigma = 2.0, T_\mu = 500, \tau = 100, N_\sigma = 10.$	$\gamma \in \{.2, .5, .8\}, \alpha \in \mathcal{L}, \sigma \in \mathcal{S}.$
ZO-SLGHd	$\beta = .001, \eta = .001, t_1 = 2.0, \gamma = .99$	$\beta \in \{.1, .001\}, \eta \in \{.1, .01, .001\}, t_1 \in \mathcal{S}, \gamma \in \{.99, .95\}.$
ZO-SLGHr	$\beta = .001, t_1 = 0.1, \gamma = .995$	$\beta \in \mathcal{L}, \gamma \in \{.999, .995\}, t_1 \in \mathcal{S}.$
ZO-AdaMM	$\beta_1 = .5, \beta_2 = .5, \alpha = 0.1, \mu = 1.0.$	$\alpha \in \mathcal{L}, \beta_1 \in \{.5, .7, .9\}, \beta_2 \in \{.1, .3, .5\}, \mu \in \mathcal{S}$
ZO-SGD	$\alpha = .1, \sigma = 1.0.$	$\alpha \in \mathcal{L}, \mu \in \mathcal{S}.$
PSO1 and PSO2	$c_1 = .2, c_2 = .8, w = .8.$	$c_1, c_2, w \in \{.2, .5, .8\}.$

Table 6: Hyper-parameters for Optimizing Rosenbrock. The candidate set for learning rates is $\mathcal{L} := \{.2, .1, .01, .001, .0001\}$. The candidate set for smoothing parameters is $\mathcal{S} := \{1.0, 2.0\}$. t_1 in ZO-SLGHd and ZO-SLGHr is the initial scaling parameter. μ in ZO-AdaMM is the scaling parameter. For EPGS and PGS, $\alpha_t = \frac{1,000\alpha_0}{1,000+t}$. The set of candidate values that lead to the minimum mean square error between the true solution and the found solution will be selected.

	Selected Values	Candidates (μ^*)
EPGS	$\alpha_0 = .2, N = 1, \sigma = 1.0.$	$N \in \{1, 2, 3\}, \alpha_0 \in \mathcal{L}, \sigma \in \mathcal{S}.$
PGS	$\alpha_0 = .1, N = 1, \sigma = 1.0.$	$N \in \{1, 3, 5\}, \alpha_0 \in \mathcal{L}, \sigma \in \mathcal{S}.$
STD-Homotopy	$\alpha = .2, \gamma = .2, \sigma = 2.0, T_\mu = 500, \tau = 100, N_\sigma = 10.$	$\gamma \in \{.2, .5, .8\}, \alpha \in \mathcal{L}, \sigma \in \mathcal{S}.$
ZO-SLGHd	$\beta = .0001, \eta = .001, t_1 = 2.0, \gamma = .999$	$\beta \in \mathcal{L}, \eta \in \{.1, .01, .001\}, t_1 \in \mathcal{S}, \gamma \in \{.99, .995, .999\}.$
ZO-SLGHr	$\beta = .0001, t_1 = 2.0, \gamma = .999.$	$\beta \in \mathcal{L}, \gamma \in \{.999, .995\}, t_1 \in \mathcal{S}.$
ZO-AdaMM	$\beta_1 = .5, \beta_2 = .5, \alpha = .2, \mu = 2.0.$	$\alpha \in \mathcal{L}, \beta_1 \in \{.5, .7, .9\}, \beta_2 \in \{.1, .3, .5\}, \mu \in \mathcal{S}$
ZO-SGD	$\alpha = .001, \sigma = 2.0.$	$\alpha \in \mathcal{L}, \mu \in \mathcal{S}.$
PSO1 and PSO2	$c_1 = .2, c_2 = .5, w = .8.$	$c_1, c_2, w \in \{.2, .5, .8\}.$

Table 7: Hyper-parameters for Figure-MNIST Attack. The candidate set for (initial) smoothing parameters is $\mathcal{S} := \{1.0, .1\}$. The hyper-parameter symbols for each algorithm are the same as their source publications. For example, t_1 in ZO-SLGHd and ZO-SLGHr denotes the initial scaling parameter, μ in ZO-AdaMM is the scaling parameter, and α denotes a constant learning rate. The number 784 equals the dimensional number d . It appears in the candidate set since it is taken from [10], who performed similar experiments. The set of candidate values that lead to the highest fitness (averaged over the 10 image attacks) are be selected.

	Selected Values	Candidates (μ^*)
EPGS	$\alpha = .1, N = .02, \sigma = .1.$	$N \in \{.01, .02, .03\}, \alpha_t \in \{.1, .05\}, \sigma \in \mathcal{S}.$
STD-Homotopy	$\alpha = .5, \gamma = .5, \sigma = 1.0,, T_{\mu} = 500, \tau = 100, N_{\sigma} = 10.$	$\gamma \in \{.5, .8\}, \alpha \in \{.5, .1\}, \sigma \in \mathcal{S}.$
ZO-SLGHd	$\beta = 10^{-4}, \eta = .001, t_1 = .1, \gamma = .995$	$\beta \in \{1/784, 10^{-4}, .1\}, \eta \in \{.1/784, 10^{-3}\}, t_1 \in \mathcal{S}, \gamma \in \{.999, .995\}.$
ZO-SLGHr	$\beta = 10^{-4}, t_1 = .1, \gamma = .995.$	$\beta \in \{10^{-4}, 1/784, .1\}, \gamma \in \{.999, .995\}, t_1 \in \mathcal{S}.$
ZO-AdaMM	$\beta_1 = .9, \beta_2 = .1, \alpha = .1, \mu = .1.$	$\alpha \in \{100/784, .001, .1\}, \beta_1 \in \{.5, .9\}, \beta_2 \in \{.1, .3\}, \mu \in \mathcal{S}$
ZO-SGD	$\alpha = 10^{-4}, \mu = .1.$	$\alpha \in \{10^{-4}, .1, 1/784\}, \mu \in \mathcal{S}.$

Table 8: Hyper-parameters for CIFAR-10 Attack. The candidate set for (initial) smoothing parameters is $\mathcal{S} := \{1.0, .1\}$. The symbols are the same as those in Table 7. The set of candidate values that lead to the highest fitness (averaged over the 10 image attacks) are be selected.

	Selected Values	Candidates (μ^*)
EPGS	$\alpha = .1, N = .03, \sigma = .1.$	$N \in \{.02, .03, .04\}, \alpha_t \in \{.1, .05\}, \sigma \in \mathcal{S}.$
STD-Homotopy	$\alpha = .5, \gamma = .8, \sigma = .1, T_{\mu} = 300, \tau = 100, N_{\sigma} = 10.$	$\gamma \in \{.5, .8\}, \alpha \in \{.1, .5\}, \sigma \in \mathcal{S}.$
ZO-SLGHd	$\beta = .01/3072, \eta = 10^{-5}, t_1 = 1.0, \gamma = .999$	$\beta \in \{.01/3072, .1\}, \eta \in \{10^{-4}/784, 10^{-5}\}, t_1 \in \mathcal{S}, \gamma \in \{.995, .999\}.$
ZO-SLGHr	$\beta = .01/3072, t_1 = .1, \gamma = .995.$	$\beta \in \{.01/3072, .1\}, \gamma \in \{.999, .995\}, t_1 \in \mathcal{S}.$
ZO-AdaMM	$\beta_1 = .9, \beta_2 = .1, \alpha = .1, \mu = .1.$	$\alpha \in \{.5/3072, .001, .1\}, \beta_1 \in \{.5, .9\}, \beta_2 \in \{.1, .3\}, \mu \in \mathcal{S}$
ZO-SGD	$\alpha = .01/3072, \sigma = .1.$	$\alpha \in \{.01/3072, 10^{-4}, .05\}, \sigma \in \mathcal{S}.$